Associations of interannual variation of Summer Tropospheric Ozone with Western Pacific Subtropical High in China from 1999 to 2017

Authors: Xiaodong Zhang[1,#], Ruiyu Zhugu[1,#], Xiaohu Jian[1], Xinrui Liu[1], Kaijie Chen[1], Shu Tao[1], Junfeng Liu[1], Hong Gao[2], Tao Huang[2], Jianmin Ma[1,*]

Affiliations:

[1]Laboratory for Earth Surface Processes, College of Urban and Environmental Sciences, Peking University, Beijing 100871, China

[2]Key Laboratory for Environmental Pollution Prediction and Control, College of Earth and Environmental Sciences, Lanzhou University, Lanzhou 730000, China

[#] These authors contribute equally to this article

[*] Corresponding author. E-mail address: jmma@pku.edu.cn (J.M. Ma).

Abstract

Associations between tropospheric ozone (O_3) and climate variations have been extensively investigated worldwide. However, given the lack of historical O_3 monitoring data, the knowledge gaps regarding the influences of climate variations on long-term O_3 trends in China remain. The present study used a tropospheric O_3 dataset from the summer of 1999 to 2017 simulated by an atmospheric chemistry model to explore the linkage between summer O_3 and a dominant atmospheric circulation system – the Western Pacific Subtropical High Pressure (WPSH) on an interannual basis in China. During this period, both WPSH strength and O_3 concentrations in eastern and central China illustrated a growing trend. An EOF analysis was conducted to examine significant summer O_3 characteristics and patterns and their potential connections with the WPSH. We find that the correlation between first principal component of summer ozone concentration in the EOF analysis and the WPSH reached 0.56 ($P \leqslant 0.01$) in China from 1999 to 2017. We show that the WPSH determines interannual fluctuations of summer O_3, whereas O_3 precursor emissions contribute primarily to the O_3 long-term trend. Our results reveal that the WPSH plays a vital role in O_3 perturbation in the

eastern seaboard regions and inland China. Precursor emissions made more significant contributions up to 60% to increasing O_3 trends in the inland urban agglomerations than coastal regions in eastern and southern China. The strongest contribution of meteorological conditions associated with the WPSH to summer O_3 occurred in the Yangtze River Delta (YRD), accounting for over 9% to ozone perturbations from 1999 to 2017. We find that the effect of the WPSH on regional O_3 depends on the spatial proximity to the WPSH. We attributed the effects of the WPSH on O_3 interannual variations to the changes in air temperature, precipitation, and winds associated with the WPSH's intensity and positions.

Keywords: tropospheric ozone, western pacific subtropical high, climate, EOF analysis

1. Introduction

Tropospheric (or surface) ozone is one of the most important components of atmospheric chemistry and is also a prominent atmospheric pollutant in China in recent years (Ma et al., 2021). Ground-level ozone pollution has overtaken $PM_{2.5}$ as the leading pollutant in many of China's urban and industrial regions (Lu et al., 2018). Surface ozone is produced through the photochemical oxidation of carbon monoxide (CO) and volatile organic compounds (VOCs) in the presence of nitrogen oxides (NO_x) and sunlight (Akimoto et al., 2015; Liu and Wang, 2020; Lu et al., 2018; Ma et al., 2021). Unlike stratospheric ozone, which absorbs harmful UV radiation that could otherwise reach the Earth's surface and cause adverse health impacts on humans, surface ozone has detrimental effects on both human health and terrestrial vegetation (Brauer et al., 2012; Fleming et al., 2018; Lefohn et al., 2017; Liu et al., 2018; Liu and Wang, 2020; Monks et al., 2015; Silva et al., 2013). In the past decade, partly due to rapid economic growth and urbanization in China, surface O_3 has increased dramatically (Maji et al., 2019; Zhan et al., 2018). Many urban areas across China have experienced growing ozone pollution, despite implementing various stringent emission

reduction measures since 2013 (Bell et al., 2014; Liu and Wang, 2020; Ma et al., 2016; Xu et al., 2016; Yan et al., 2013).

Surface ozone formation and evolution rely on meteorology, atmospheric chemistry, and the emissions of O_3 precursors, such as VOCs and NO_x emitted from fuel combustion (Li et al., 2020; Ma et al., 2021). Meteorological parameters affecting surface O_3 evolution include but are not limited to winds, air temperature, relative humidity, and solar radiation (Ma et al., 2021). While anthropogenic factors play vital roles in ozone formation, meteorological factors determine, to a significant extent, the changes and evolution in O_3 concentrations (Ding et al., 2019; Li et al., 2019, 2020; Lin et al., 2021, 2022). Meteorological conditions modulate O_3 concentrations through atmospheric transport and affect natural emissions from biological sources and chemical reaction rates (Fu et al., 2019; Li et al., 2020; Lu et al., 2019). Extensive investigations have been devoted to short-term, such as hourly and diurnal changes in O_3 levels and their associations with meteorological conditions (Dang et al., 2021; Han et al., 2020). Given the strong connections between O_3 concentration and air temperature, atmospheric humidity, and winds, interannual and longer-term variations of O_3 are also elucidated in China and worldwide (Chen et al., 2020; Li et al., 2020). Daily and interannual variations of summertime surface O_3 have been linked with atmospheric teleconnection patterns, such as the ENSO (El Niño-Southern Oscillation), East Asian summer monsoon, and the WPSH (Liu et al., 2019a; Wang et al., 2016; Yang et al., 2022; Yihui and Chan, 2005; Yin et al., 2019; Zhao and Wang, 2017; Zhou et al., 2009). These climate teleconnection patterns provide dynamic and thermodynamic backgrounds of regional and large-scale weather systems that could markedly affect the atmospheric pressure, temperature, and winds. Using modeled summer O_3 time series across China from 1999 to 2017, we have examined the response of gridded summer O_3 concentrations to the East Asian Summer Monsoon Index (EASMI), Nino indices, and western North Pacific subtropical high index (WPSH-I), the three climate modes influencing significantly the summer weather and climate in China, on an annual basis in the six major UAs in China (Zhang et al., 2022). The correlation coefficients between the summer O_3 concentrations and the three climate

modes from 1999 to 2017 are 0.54 (WPSH-I, p=0.016), 0.38 (Nino indices, p=0.105), and 0.27 (EASMI, p=0.267), respectively. The results revealed that interannual changes in summer O_3 averaged over these UAs were more significantly associated with the WPSH-I among three atmospheric teleconnection patterns. The finding motivates us to carry out more broad and deep investigations of the associations between the long-term change in summer O_3 and the WPSH, aiming to shed new light on the extent of the impact of climate variation on O_3 trends in urban China.

Limited studies have been carried out to examine the linkage of summer O_3 in China with the WPSH (Jiang et al., 2021; Yin et al., 2019; Zhao and Wang, 2017; Liu et al., 2019a). These studies all focused on the response of daily and short-term summer O_3 variation to the WPSH in eastern China using measured O_3 concentrations within a short period (e.g., 2015-2018, Yin et al., 2019). The common conclusions of these studies were that stronger WPSH tended to increase daily surface ozone concentration over northern China but reduce it over southern China, which was partly attributed to a stronger southwesterly transport of moisture into Southern China that was not conducive to ozone formation. However, the associations between interannual or longer-term variations of WPSH and interannual or longer ozone trends in mainland China are almost unknown. To fill this knowledge gap, we performed multiple atmospheric chemistry model simulations of summer (June, July, and August) O_3 concentrations across China from 1999 to 2017. This O_3 dataset enables us to explore the responses of the long-term trend and interannual variation of O_3 concentrations to climate variations and to take a broader look at the associations between ozone evolution and the Western Pacific subtropical high in China (Zhang et al., 2022).

2. Methodology

2.1. WRF-Chem Model Configuration

The Weather Research and Forecasting model coupled with Chemistry (WRF-Chem) v3.7 (http://www2.mmm.ucar.edu/wrf/users/wrf_files/wrfv3.7/updates-3.7.html) was employed to quantify the influences of the WPSH on O_3 variation in

China. The model covers mainland China with a 20 km × 20 km grid resolution, extending from the ground surface to 50 hPa with 30 non-uniformly distributed vertical layers (Zhang et al., 2022). Anthropogenic emissions data of atmospheric pollutants from 1998 to 2017 were collected from EDGAR (Emissions Database for Global Atmospheric Research) v4.3 (https://edgar.jrc.ec.europa.eu/), including gridded annual emission data for CH_4, BC, OC, NH_3, NMVOC, NO_x, CO, SO_2, and primary PM_{10} and $PM_{2.5}$. The biogenic emissions were estimated by the MEGAN v2.1 (Model of Emissions of Gases and Aerosols from Nature) (Guenther et al., 2012). Detailed WRF-Chem configuration, modeling setup, and precursor emissions are referred to by Zhang et al. (2022). WRF-Chem model was integrated to predict daily O_3 concentrations in summer (June to August) from 1998 to 2017. After excluding the model spin-up time, the O_3 time series from 1999 to 2017 was used in the present study. The daily concentrations were summed and averaged over the summer season to obtain mean O_3 concentrations. The modeled O_3 concentrations were verified by measured daily O_3 concentration data in several major UAs across China from 2016 to 2017. The results show better agreements between modeled and sampled O_3 air concentrations. Details are referred to in Supporting Information Text 1, **Fig. S1** and Zhang et al (2022).

2.2. WPSH index

The WPSH is an anticyclonic system hovering over the middle and lower troposphere of the northwestern Pacific Ocean. The WPSH forms during the summer months and dissipates in winter. As a high-pressure system, the WPSH is associated with stable weather conditions featured by high temperature and low rainfall. These weather conditions, in turn, perturb significantly O_3 variation. While varying year from year, the WPSH in summer generally covers much of East Asia, including parts of China, Japan, and the Korean Peninsula. It can also extend westward, affecting Southeast Asia, including Vietnam, Thailand, and the Philippines (Jiang et al., 2021; Yang et al., 2022). Although the summer WPSH determines primarily the weather and climate conditions in Eastern and Southern China, it may also influence the weather

systems in Western and Northern China. For example, the westward and northward movement of the WPSH might lead to a weak high-pressure system in Northern Xinjiang extending to Central-North China, resulting in higher temperatures and lower rainfall in this region, whereas a low-pressure system could prevail in Northern and Northeastern China, enhancing precipitation in this part of China. However, given lower O_3 levels in Westernmost China (Tibet and Xinjiang), the present study did not attempt to elucidate the associations between O_3 evolution and the WPSH in this part of China but focused on Central and Eastern China where significantly higher O_3 levels were observed.

The WPSH indices were collected from the National Climate Center of China (NCCC, the WPSH index is available at http://cmdp.ncc-cma.net/download/precipitation/diagnosis/NWP_high/wpsh_idx.txt). The NCCC reports four WPSH indices, including the WPSH area index, intensity index, the westernmost point, and the ridgeline index of the WPSH. These indices define and quantify the changes in the WPSH via its size, intensity, east–west expansion, and north–south movement (Liu et al., 2019b). These WPSH activities significantly affect China's daily, seasonal, interannual, and longer-term meteorological fields and climate variations. Among the four WPSH indices, we found that the WPSH area index (hereafter referred to as WPSH-I1) exhibited the most significant positive correlations with modeled summer ozone concentrations in most regions of China. Since summer rainfall in China was reported to be more sensitive to the western ridge point of the WPSH (Jiang et al., 2021; Yang et al., 2022; Zhao and Wang, 2017), which might affect the O_3 wet deposition, we also considered the westernmost point of the WPSH (hereafter referred to as WPSH-I2) in the present study. We found the strongest negative correlations between O_3 concentrations and WPSH-I2, which is likely associated with O_3 washout by precipitation. In light of this, we chose the WPSH-I1 and WPSH-I2 to elucidate the potential influences of the WPSH on the interannual variations of WRF-Chem simulated summer O_3 concentrations for the past two decades. As shown in **Fig. S2**, the WPSH strength characterized by the WPSH-I1 index illustrates a growing trend after 1999, suggesting the reinforcement of the WPSH on a

decadal scale in the recent two decades, the period coincident with the most rapidly growing O_3 pollution in China. This growth trend of the WPSH possibly overwhelms interannual changes in the WPSH.

2.3. O_3 and meteorological data

Surface O_3 concentration data on a daily basis used the WRF-Chem simulated concentration data (section 2.1). Meteorological data used the WRF predicted gridded air temperature (C^o), 500-hPa geopotential height (GH, ghm), winds (m s^{-1}), the sea surface pressure (SSP, hPa), and incoming solar radiation flux (W m^{-2}). To reduce uncertainties from WRF predicted meteorological data in the composite analysis for examining the responses of interannual variation of summer ozone to the WPSH, we also collected NCEP reanalysis data based on meteorological observations, including geopotential height at the 500 hPa, the surface air temperature (SAT, ^oC), and precipitation from NCEP reanalysis (https://psl.noaa.gov/data/reanalysis/reanalysis.shtml). These data were used to illustrate the characteristics of meteorological fields during the positive and negative phases of WPSH indices and in the first EOF loadings, which will be elaborated on below.

2.4. EOF analysis

To extract the potential influences of the interannual changes in the WPSH on O_3 variations, we conducted the EOF analysis and examined associations between meteorological fields and surface O_3 from 1999 to 2017. The empirical orthogonal function (EOF) analysis as a multivariate statistical technique has been extensively used in atmospheric science to explore the spatiotemporal variations in a meteorological variable or air pollutant (Fiore et al., 2003; Pu et al., 2016; Shen et al., 2015; Yin et al., 2019; Zhao and Wang, 2017). In the present study, we used the EOF analysis in WRF-Chem simulated gridded (20 km × 20 km) seasonal O_3 concentrations across China to extract annual O_3 change features from 1999 to 2017. The EOF analysis of the O_3

concentration time series from modeled data was designed to investigate potential associations between the summer O_3 time series and WPSH and to explore the response of the O_3 time series to increasing WPSH strength since 1999. The orthogonal modes included spatial and temporal coefficients and contained information of some proportion (variance contributions) from the original fields.

2.5. Model scenario setup

We quantify the contribution of meteorology and precursor emissions to O_3 evolution subject to WPSH by setting up three model scenarios. Considering the increasing trend of the WPSH from 1999 onward, we integrated WRF-Chem from 1998 to 2017, subject to three model runs. The first model scenario run took the variable meteorological field and annual O_3 precursor emissions from 1998 to 2017, with 1998 as the model spin-up period, referred to as the base scenario (scenario 1); the second scenario run adopted fixed precursor emissions in 1998, but variable meteorology throughout 1998 to 2017, referred to as model scenario 2, and the third scenario implemented fixed meteorology in 1998 but variable precursor emissions, referred to as model scenario 3. The simulated O_3 concentrations from these three scenarios were compared to identify the relative significance of meteorology and precursor emissions in the changes in O_3 concentrations.

3. Results and Discussion

3.1. EOF analysis

Figures 1a and **1b** show modeled summer mean O_3 concentrations and standard deviations (STD) averaged from 1999 to 2017. Higher concentrations are observed in Sichuan and the region extending from central China to the Northern China Plain (NCP), rather than the southern and southeastern seaboard areas where O_3 pollution has been receiving extensive concerns (**Fig. 1a**). This spatial distribution pattern agrees well with measured mean summer concentrations data averaged from 2015 to 2017 in China (**Fig.**

S3). The STD distribution does not superimpose with O_3 concentrations but is centered in the Sichuan Basin and those provinces in the middle reaches of the Yangtze River, implying that O_3 fluctuated more strongly by interannual variations of meteorological fields in this region.

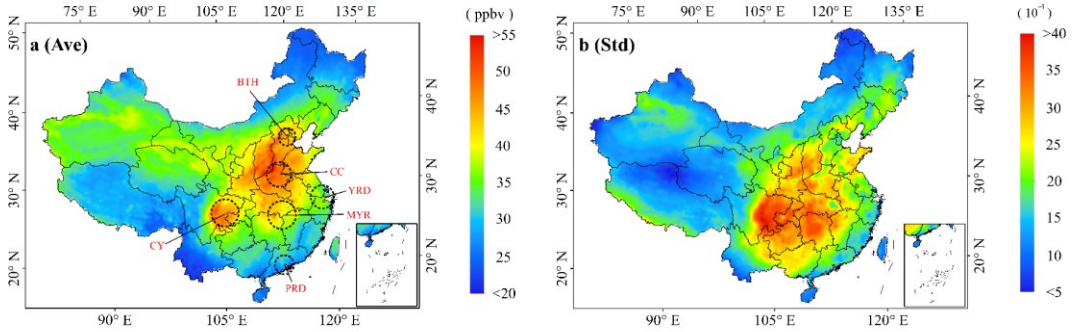

Figure 1. Mean summer O_3 concentrations (**a**) and standard deviations (**b**) averaged from 1999 to 2017.

We carried out an EOF analysis by using summer O_3 as the original field to illustrate the spatiotemporal variation of O_3 in China on an annual basis from 1999 to 2017, aiming to explore the response of summer O_3 interannual (1999 to 2017) variation to the WPSH, the period matching the significantly increasing trend of the WPSH-I1 (Supporting Information (SI), Inset figure of **Fig. S2**), which may lead to a more robust response of the O_3 time series to the WPSH. The results of the first and second EOF patterns for both periods are presented in **Fig. 2**. Each EOF spatial pattern represents a share of the total variation of surface ozone proportional to its eigenvalue. The first EOF loadings (PCA1) are associated strongly with the mean summer O_3 concentrations averaged over the six UAs in China at the correlation coefficient of 0.95 ($p<0.01$) from 1999 to 2017. The EOF1 pattern also illustrates similarities with the mean summer O_3 concentrations and its standard deviations (**Fig. 1a** and **1b**), featured by large values in central China. Differing from the EOF1, the EOF2 patterns show a south-north contrast pattern. During this period, the first EOF pattern (EOF1) explains 67.4% of the total variance in summer O_3, and the second EOF pattern (EOF2) explains 9.7% of the total variance. The negative and positive values in the EOF patterns are expected to represent the extent of departures from the average summer ozone. Since the EOF1 pattern is the

maximum possible fraction of the variability in the original data, in our case, it explains most of the summer O_3 variability, featured by the growing trends of summer O_3 concentrations. The EOF1 pattern appears to agree, to a large extent, with measured summer (June to August) and warm season (April to September) MDA8 (maximum 8h average) O_3 distribution (Lu et al., 2018; Liu, 2020). The EOF2 patterns also agree with the second EOF pattern that Yin et al. (2019) obtained, though their EOF analysis focused on daily O_3 in eastern China. The result suggests that the NCP suffered from higher O_3 pollution and was also subject to O_3 evolution during the past decades.

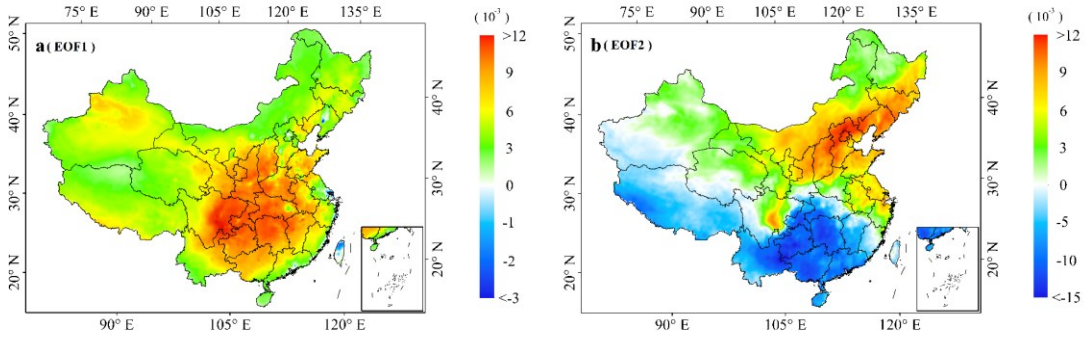

Figure 2. First (a) and second (b) EOF patterns across China from 1999 to 2017.

The EOF1 shown in **Figs. 2a** suggests that the most significant variations in summer O_3 occurred in inland areas of China, extending from Sichuan Province to the middle and lower reaches of the Yangtze River and from Hunan to Shanxi Province. This inland region covers several major UAs in China, including Central China (CC), Middle Reaches of the Yangtze River (MYR), and Chengyu (CY, Chengdu−Chongqing) urban agglomeration (Zhang et al., 2022). We estimated the correlation coefficients between the first EOF loading (PCA1) and summer O_3 concentrations in the six UAs, where 34.3% of China's population resides. The results are presented in **Fig. S4**. Strong statistically significant correlations were found in CC ($r = 0.86$, $p<0.01$), CY ($r = 0.92$, $p<0.01$), and MYR ($r = 0.90$, $p<0.01$). Whereas, in the other three UAs located near the coastal regions, namely the YRD, PRD, and BTH, the correlation coefficients range from 0.36 to 0.51 (**Fig. S4**). In particular, the PCA1 exhibits more strong association with the summer O_3 anomalies averaged over the six UAs, reaching r=0.94 (p<0.01).

The good correlations between O_3 concentrations and PCA1 are expected because, as aforementioned in section 3.1 that, the EOF analysis was carried out by using summer O_3 concentrations as the original field that have been increasing during the past decades. However, the magnitude of the correlation coefficients helps identify the extent of O_3 pollution and long-term growth trends in China and different UAs (or regions). Overall, these results confirm a more substantial interannual variation of summer O_3 in the inland areas than in coastal regions of southern and southeastern China.

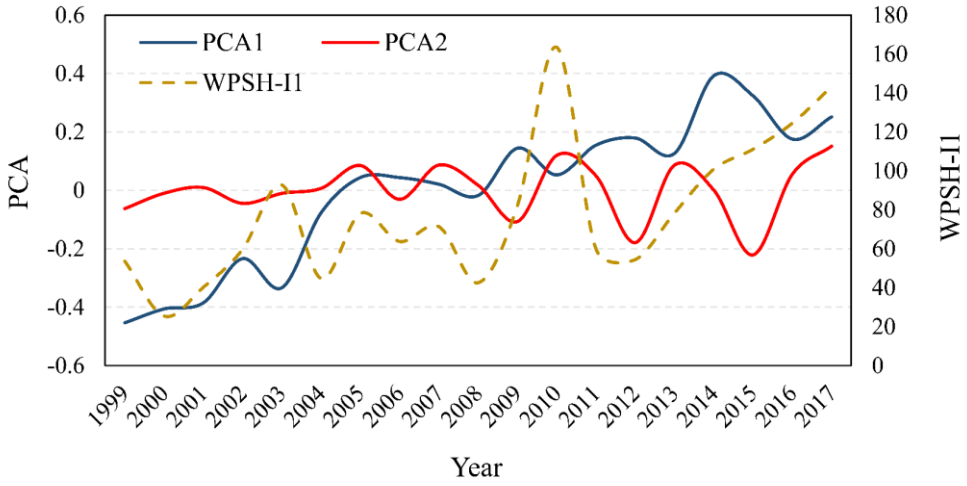

Figure 3. Annual variation of two EOF loadings (PCA1 and 2, scaled on the left Y-axis) and WPSH-I1 (dashed brown line, scale on the right Y-axis) from 1999 to 2017.

Figure 3 shows annual variations of the two EOF loadings (PCA1-2), scaled on the left Y-axis) and the WPSH-I1 (dashed brown line, scaled on the right Y-axis) from 1999 to 2017. The first EOF loading (PCA1) and WPSH-I1 exhibit growing trends during this period with a correlation coefficient of 0.56 ($p<0.01$). PCA2 shows no clear trend and hence is not associated with WPSH-I1. The increasing trend of WPSH-I1 since 1999 likely anticipates the interdecadal variation of the WPSH for the recent two decades. Since O_3 concentrations are positively correlated with the WPSH-I1 (**Figs. 3** and **4**), stronger WPSH intensity might elevate summer O_3 levels in China on an annual basis, particularly the areas with large EOF1 values in inland China (**Fig. 2a**). However, this conclusion is not well applicable in the PRD region, where we observed the lowest association between the EOF1 and summer O_3 concentrations (**Fig. 2**) and between the

WPSH-I1 and O_3 levels among the six UAs and over China (**Fig. S4**). It is also worthwhile to note that, because O_3 precursor emissions in China have been growing during the past two decades and modeled concentrations were mainly attributed to precursor emissions, the positive correlations between O_3 concentrations and the WPSHI-I1 should not be understood that the WPSH drove elevated O_3 for a long term perspective. Further discussions are provided in the next section.

We further compared the 500-hPa geopotential heights (GH, gpm) anomalies in the positive and negative phases of PCA1 and WPSH-I1 as the departure from their respective means averaged from 1999 to 2017. We selected those years with the positive and negative anomalies of the PCA1 and WPSH-I1 $\geq \pm 1$ standard deviation (STD, referred to as the positive and negative phase hereafter) and then estimated their composite means. The results are shown in **Figs. S5** and **S6**. It can be seen that the composite means of 500-hPa geopotential height in the positive and negative phases of the PCA1 and WPSH-I1 illustrate good spatial similarities, again demonstrating the connections between summer O_3 and WPSH-I1. In the positive phase, positive geopotential height anomalies at the 500-hPa governed China, except for the NCP regions, including the BTH urban agglomeration, where negative anomalies of the 500-hPa geopotential heights are observed. On the other hand, a south-north contrast pattern of the geopotential height composite anomalies is discerned in the negative phase of the PCA1 and WPSH-I1. The spatial patterns of GH composite anomalies in the positive and negative phases of the EOF1 also exhibit some similarities with the GH composite anomalies based on positive and negative O_3 concentration anomalies as the departure from mean O_3 levels averaged over the six UAs in China from 1999 to 2017 (**Fig. S6**).

3.2. Associations of summer O_3 with WPSH

Having established the relationships between summer O_3 and WPSH via the EOF analysis, we further explore the direct responses of summer O_3 to WPSH. Since the effects of the WPSH span vast regions, and the changes in surface ozone concentrations

may be influenced by the variations in meteorological factors associated with the WPSH, a spatial correlation analysis between summer surface ozone concentrations in China and WPSH (WPSH-I1) index from 1999 to 2017 was conducted. The result is illustrated in **Fig. 4**. During this period, positive correlations overwhelm mainland China, except for the PRD region (**Fig. 4)**. The summer O_3 level in the PRD was the lowest among the six UAs (**Figs. 1** and **S3**). The causes of the lack of statistically significant O_3 trend and negative correlation between WPSH-I1 and O_3 in the PRD might be complex. The stronger WPSH and its westward extension can yield high temperature and dry weather condition in the PRD, which is conducive to elevated O_3 concentration, and vice versa. **Figure S7** shows relatively strong positive correlation between SAT and WPSH-I1, which favors growing O_3 concentrations, and negative correlation between precipitation and WPSH-I1 precipitation, which removes O_3 concentrations from air in the PRD region. From the early 2000s, Hong Kong and Guangdong provincial governments jointly lunched an O_3 pollution control program, which significantly reduced O_3 precursor emissions and its atmospheric levels in the PRD (Wu et al., 2013). It is likely that the course of O_3 reduction in the PRD coincided with the period of our modeling investigation, which interferes the statistical correlation between WPSH and O_3 in the PRD.

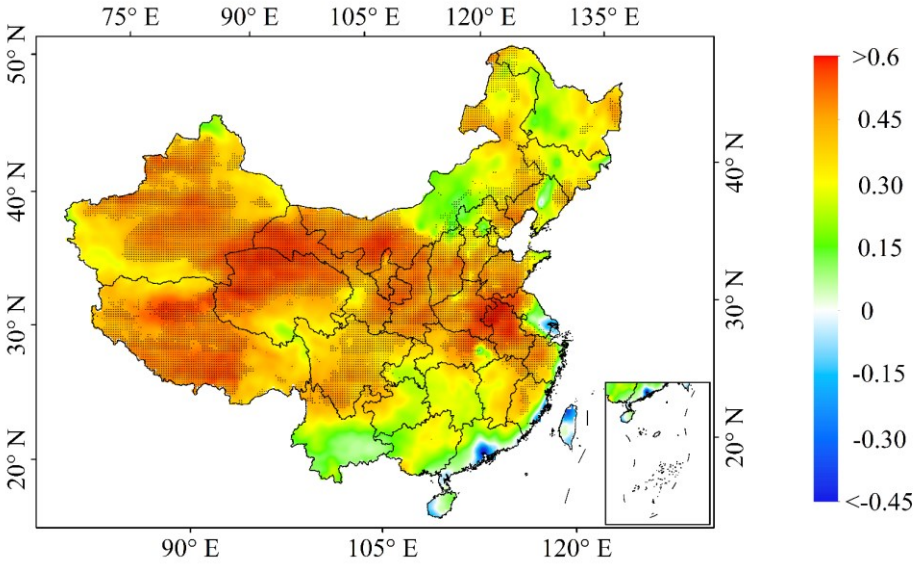

Figure 4. Correlation coefficients between summer O_3 concentrations and WPSH-I1 across China from 1999 to 2017 on the interdecadal scale under model scenario 1. The areas filled with black dots indicate the regions where the correlation is statistically significant ($p<0.05$).

Considering that summer precipitation in China is sensitive to the western ridge point of the WPSH (Jiang et al., 2021; Yang et al., 2022; Zhao and Wang, 2017), we also examined the responses of meteorological fields to the changes in the western ridge point index of the WPSH (referred to as the WPSH-I2) subject to its positive and negative phases. The WPSH-I2 is opposite to the WPSH-I1 (**Fig. S8**). We estimated WPSH-I2 anomalies as the departure from its mean from 1999 to 2017. We defined the positive WHSH-I2 phase if its values are greater than one standard deviation and the negative phase if WHSH-I2 < one standard deviation. The annual summer mean meteorological variables in the positive and negative phases of the WHSH-I2 are summed to obtain their respective composite means. We then calculated the anomalies of these composite means by subtracting their respective long-term means averaged from 1990 to 2022. **Figure 5** shows the anomalies of composite means of 500-hPa GH, precipitation (cm/mn), and the surface air temperature (SAT, ^{o}C) across China in the positive and negative phases of WPSH-I2. The results identified evident north-south contrast for all three meteorological variables in the positive phase of the WPSH-I2. Of which, the anomalies of GH composite means are positive in northern China with a center in Mongolia and northeastern China (**Fig. 5a**). In contrast, the broad region to the south of 35^{o}N is under the regime of negative GH composite anomalies (**Fig. 5b**). The 500-hPa GH patterns can also be confirmed by the anomalies of composite mean sea level pressure (SLP) in the positive and negative phase of WPSH-I2 (**Fig. 6**), showing negative SLP anomalies from the Bay of Bengal to the tropical western Pacific in the positive phase of the WPSH-I2 and positive anomalies covering a vast region from southeast to northeast China. The south-north dipole patterns of 500-hPa GH composite anomalies in **Fig. 5a** and the SLP composite anomalies in **Fig. 6** often accompany the termination of the rain season in southern China and the start of the rainy season in northern China (Nie et al., 2021), as shown by the negative rainfall anomaly in southern China and positive anomaly in northern China. **Figure 5a** predicts

the weakening WPSH or the northward movement of the WPSH, leading to a southward pressure gradient, as shown in **Fig. 5a**. As a result, the composite anomalies of 850-hPa vector winds illustrate northerly wind components over central-south and southern China (**Fig. 6**). Such northerly wind anomalies do not favor southward water vapor transport by southwesterly Indian monsoon.

On the other hand, easterly and southeasterly wind components extend from tropical west Pacific to central and northern China, paving a water vapor transport pathway and corresponding to the positive rainfall anomaly in this part of China (**Fig. 5c**). In the negative phase of the WPSH-I2, positive SLP anomalies overwhelmed eastern China with a center in the coastal region of southern China, implying the enhancement of the WPSH. Accordingly, we observe negative composite anomalies of the precipitation extending from the Yangtze-Huaihe Valley from central to northeastern China, suggesting declining precipitations in these regions. Growing precipitations are seen in southern and southeastern China, characterized by the positive composite anomalies of the precipitation (**Fig. 5c**).

Precipitations in China have been connected strongly with the WPSH-I2 from a daily perspective (Duan et al., 2008; Nie et al., 2021). Along with the westward shifting of the WPSH ridge point, the major rain belt moves northward to the middle and lower reaches of the Yangtze River from June to mid-July and northern and northeastern China from late July to mid-August (Lu et al., 2017; Su et al., 2014; Zhao and Wang, 2017). In our case, with the focus on the association between summer O_3 and WPSH from the interannual perspective, we show that the growing summer rainfall in southern and southeastern China is associated with stronger WPSH in an east position, featured by negative GH composite anomalies to the south of 35°N in China (**Fig. 5a**). Such GH anomaly pattern does not favor atmospheric water vapor transport to North China by the summer monsoon circulations (Nie et al., 2021), which results in low rainfall in this part of China (**Fig. 5c**). Accordingly, relatively higher SATs are observed in North China (**Fig. 5e**), which, together with low atmospheric humidity and rainfall, favors O_3 formation and evolution. On the other hand, the stronger rainfall in southern and southeastern China caused lower SATs in this region, characterized by negative SAT

412 composite anomalies (**Fig. 5e**). The higher atmospheric humidity, stronger rainfall or
413 precipitation washout, and lower SATs tend to restrain O_3 formation in southern China,
414 which resulted in lower O_3 levels compared to that measured in central and northern
415 China (Lu et al., 2018; Liu, 2020). This is likely a reason for higher O_3 concentrations
416 observed in northern and central-north China, such as the BTH and central China urban
417 agglomerations, than in YRD and PRD regions. In the negative phase of the WPSH-I2,
418 the north-south contrast pattern of all three meteorological variables vanished. Instead,
419 positive GH composite anomalies at the 500-hPa are seen in China, with more muscular
420 positive anomalies in western Mongolia (**Fig. 5b**). Such GH pattern suggests the
421 reinforcement and western shift of the WPSH. As a result, the composite anomalies of
422 the summer precipitation in northern China turned to positive, meaning high rainfall in
423 this region (**Fig. 5d**). However, the composite anomalies of SATs in the negative phase
424 of the WPSH-I2 (**Fig. 5f**) seem not to respond well to the intense rainfall, except in the
425 PRD, where declining SATs, featured by the negative SAT composite anomalies (**Fig.**
426 **5f**), corresponding well to the positive composite precipitation anomalies, meaning high
427 rainfall in this region (**Fig. 5d**). This result also is in line with previous observations
428 that the westward shift of the WPSH ridge point often accompanied with the
429 termination of the systematic rainfall in southern China (Duan et al., 2008; Huang et
430 al., 2018; Nie et al., 2021).
431

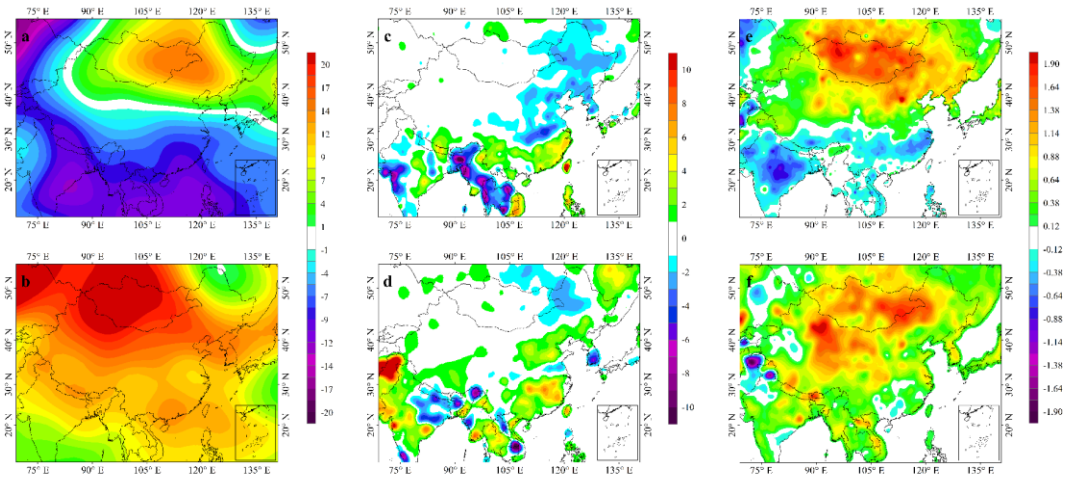

432

Figure 5. Anomalies of composite means of 500-hPa GH (GPH) in positive (**a**) and negative (**b**) phase of WPSH-I2 from 1999 to 2017; same as Fig. 5a and 5b but for precipitation (cm/mn) in positive (**c**) and negative (**d**) WPSH-I2 phase; same as Fig. 5a and 5b but for SAT (°C) in positive (**e**) and negative (**f**) phase of WPSH-I2 from 1999 to 2017.

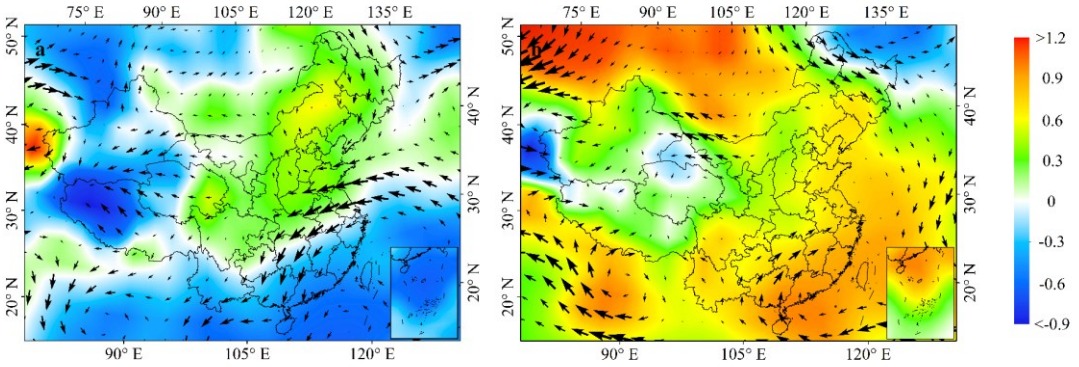

Figure 6. Anomalies of composite means of sea level pressure (SLP, hPa) overlapped with the anomalies of composite mean 850-hPa vector winds across China in the positive (**a**) and negative (**b**) phases of WPSH-I2 from 1999 to 2017.

3.3. WPSH and interannual O_3 fluctuations

Having identified the associations between the WPSH and O_3 evolution on interannual scales, it is also interesting to know to what extent the WPSH could contribute to the interannual fluctuations in O_3 concentrations in China and its major UAs. We compared modeled O_3 concentrations among three model scenarios by estimating their differences (fractions). **Figure 7** illustrates summer mean O_3 concentrations averaged from 1999 to 2017 from the three scenarios. Identical concentration spatial patterns can be observed in scenarios 1 (base, **Fig. 7a**) and 3 (fixed meteorology, **Fig. 7c**), suggesting that precursor emissions overwhelmed the spatial-temporal distribution of summer ozone in China. Comparing **Figs. 7b** with **Fig. 7a** and **7c**, we also notice that the low summer ozone levels simulated from model scenario 2 (fixed precursor emissions, **Fig. 7b**) extend a much larger area across southern China (highlighted by a solid red circle). Considering that model scenarios 1 and 2 used the same meteorological data from 1998 to 2017, the lower O_3 levels under scenario 2 can be attributed mainly to declining precursor emissions, partly attributable to a collaborative effort to mitigate air pollution in the PRD and Hong Kong since the early

2000s as aforementioned before, which effectively slowed down growing O_3 precursor emissions (Wu et al., 2013).

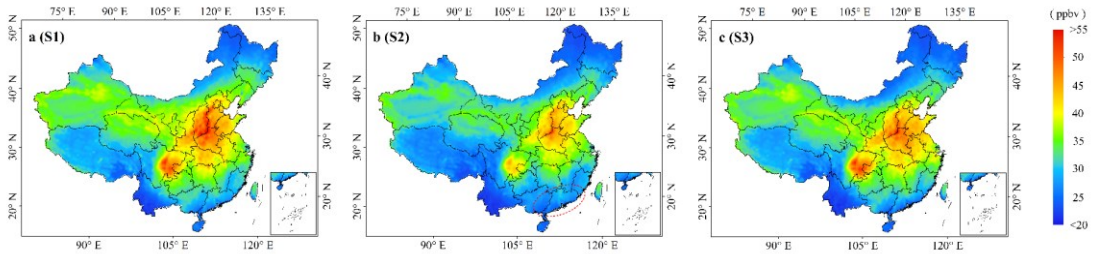

Figure 7. Modeled mean summer O_3 concentrations across China averaged from 1999 to 2017: (a) Model scenario 1 (base scenario), (b) model scenario 2 (fixed precursor emission), and (c) model scenario 3 (fixed meteorology).

To extract signals of meteorology in modeled O_3 concentrations, we calculated the percentage change in summer O_3 concentrations subject to model scenarios 1 and 3, defined as $O_{3,frac} = (O_{3(S3)}-O_{3(S1)})/O_{3(S1)} \times 100\%$, where $O_{3(S3)}$ and $O_{3(S1)}$ represent the summer ozone concentrations for scenarios 3 and 1 between 1999 and 2017 (**Fig. 8a**). Since both model scenarios 1 and 3 used the same precursor emissions, their differences (fractions) can quantify the meteorological effect on O_3 fluctuations. Significantly, the WPSH was at a relatively high value in 1998 compared to 1999-2017 (**Fig. S2**). The result shows that the fixed meteorological conditions (scenario 3) resulted in higher summer ozone concentrations in the eastern seaboard region of China than the results from the base scenario, particularly in the YRD, where the fixed meteorological conditions enhanced the summer concentration by >9% compared to the base scenario modeling result (**Fig. 8a**). The second-highest O_3 fraction between the scenarios 1 and 3 occurred in the Sichuan Basin, where the scenario 3 predicted the summer concentrations are 3% to 6% higher than the base scenario 1. **Figure 8b** presents the correlation coefficients between the WPSH-I1 and scenario 2 modeled O_3 concentrations across China from 1999 to 2017, showing relatively high positive correlation coefficients in the eastern seaboard area and the region extending from the Sichuan Basin to the Gansu-Shaanxi border, like the fractional changes shown in **Fig. 8a**. However, the negative correlations extended in most parts of China, indicating that

the WPSH tends to reduce summer O_3 levels in these regions. This spatial correlation pattern differs significantly from the correlation pattern shown in **Fig. 4**, in which positive correlations between the summer WPSH and modeled O_3 under the base scenario almost extend entire China. As aforementioned, this is because both WPSH-I1 and O_3 precursor emissions in China increased from 1999 to 2017. **Figure 8** shows some similarities between spatial distribution patterns of the fractional changes in summer O_3 concentrations under scenarios 1 and 3 and the correlations of summer O_3 concentrations from model scenario 2 and the WPSHI-I1. The result suggests that the meteorological conditions contributing to summer O_3 evolution, as shown in **Fig. 8a**, are associated, to a large extent, with the WPSH. The positive contribution of meteorology characterized by the positive correlations to elevated O_3 pollution gradually weakens in inland areas and turns into a negative contribution, meaning the reduction of summer O_3 by meteorology in inland China, including most northern and northeastern regions. Although positive correlations were estimated in the Tibet Plateau, given very low O_3 pollution, the WPSH would not exert any significant influence on O_3 levels in the plateau. It is worth noting that **Figure 4** shows a negative correlation between modeled summer O_3 concentration from model scenario 1 and WPSH-I2 time series in the YRD but model scenario 2 yields a positive correlation (**Fig. 8b**). Since model scenario 1 took annually-altered O_3 precursor emissions into consideration, the negative correlation suggests that declining precursor emissions from 1999 to 2017 in the YRD overwhelmed the WPSH effect. After removed the effect of precursor emissions, the meteorological conditions associated with the WPSH would help enhance O_3 concentrations in this region.

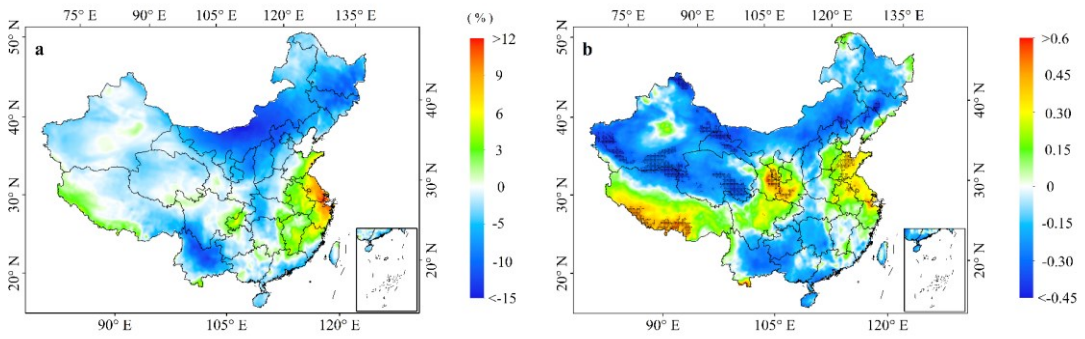

Figure 8. Fractional changes between modeled O_3 concentrations subject to model scenarios 3 and 1 from 1999 to 2017 estimated by $O_{3,frac} = (O_{3(S3)}-O_{3(S1)})/O_{3(S1)} \times 100\%$ (a), and correlation coefficients between summer WPSH-I1 and modeled summer O_3 concentrations under model scenario 2 (b). The areas filled with black dots in **Fig. 8b** indicate the regions where the correlation is statistically significant ($p<0.05$).

As shown in **Fig. 5c,** the positive WPSH-I1 corresponds to lower precipitation in southern and southeastern China and higher precipitation in central and northern China, which tends to enhance O_3 levels in southern and southeastern China and reduce O_3 concentrations in the north. Although we also observe higher SATs across northern China and lower SATs in the south, which should increase O_3 levels in the north and decrease O_3 levels in the south, we could not quantify the direct linkages between SATs and O_3 concentrations from a national perspective. **Figure S7** displays the correlation coefficients between summer WPSH-I1 and the SAT (**Fig. S7a**) and precipitation (**Fig. S7b**) from 1999 to 2017 across China. We can observe stronger positive correlations between the WPSH-I1 and SAT in southern China, indicating that the WPSH tends to enhance SAT in this region. This should favor elevated O_3 concentrations instead of the reduction of O_3 levels, as shown in **Fig. 7b**. This result likely anticipates that stronger precipitation associated with WPSH in this part of China overwhelmed SAT and overall yielded lower O_3 concentrations in southern China. Considering strong association of O_3 formation and solar radiation (sunlight), we also estimated the correlation coefficients between surface incoming solar radiation flux (W m^{-2}) and O_3 concentration and WPSHI-I1 from 1999 to 2017 across China. The results are illustrated in **Fig**. **S9**. The spatial pattern of the correlation coefficients between the radiation flux and O_3 concentration is similar to the correlation between SAT and WPSH-I1 with higher correlations across the China's eastern and southern seaboard regions (**Fig. S9a**), implying that O_3 should be more readily formed in these regions, though O_3 levels were not higher in these regions than Central China and the BTH (**Fig. 1**), as discussed below. However, no statistically significant positive correlations between radiation flux and WPSH-I1 were identified (**Fig. S9b**)

Figure S10 illustrates annual variations of summer averaged O_3 concentrations under the three model scenarios from 1998 to 2017 over six UAs. Distinct differences between the three inland UAs (CY, CC, and MYR) and the three coastal UAs (YRD, PRD, and BTH) can be discerned from more significant fractions with an increasing trend in CY, CC, and MYR, as compared to YRD, PRD, and BTH, in which there were no significant trends in modeled concentrations. In the three inland UAs (CY, CC, and MYR, **Fig. S10d-f**), O_3 concentrations under fixed precursor emissions (scenario 2, solid red line) are lower markedly than that from scenario 1(solid green line) and exhibit no statistically significant temporal trend, suggesting that the variable meteorology does not contribute significantly to O_3 levels and its long-term temporal trends. On the other hand, O_3 concentrations under scenarios 1 and 3 runs are more or less similar and illustrate increasing trends, indicating that growing precursor emissions in the past two decades dominate long-term O_3 evolution in these inland UAs. In the three coastal UAs (PRD, YRD, and BTH), the increasing trends of modeled summer O_3 under scenario 3 were less significant than in the three inland UAs, indicating slower growth of precursor emissions in these coastal UAs. No significant increasing trends of O_3 concentrations from scenario 3 run (fixed emission in 1998) are observed, suggesting that the changes in meteorological conditions in the past two decades contributed less to growing O_3 pollution in China's major urban clusters than precursor emissions. However, we noticed from **Fig. S10** that annual fluctuations of summer O_3 concentrations in these UAs under scenario 2 agree, to a large extent, with the results from model scenario 1 (base scenario). This is expected because the two model scenarios shared the same meteorology. As a result, precursor emissions contributed primarily to the long-term O_3 growing trends and magnitudes, whereas meteorology made more vital contributions to interannual fluctuations of O_3 concentrations.

To link the interannual fluctuations of summer ozone induced by meteorology with WPSH, we estimated the rate of interannual variation (RIV) of summer O_3 concentrations simulated by model scenario 2 in the 6 UAs and WPSH-I1, given by $C_r = [c(n) - c(n\text{-}1)]/c(n\text{-}1) \times 100\%$, where $c(n)$ and $c(n\text{-}1)$ are summer O_3 concentrations in the current year and previous year, respectively. The same approach also calculated the

570 RIV of summer WPSH-I1. **Figures 9a** and **9b** present the RIV of summer O_3
571 concentrations in the three inland and coastal UAs, respectively. The RIV of the WPSH-
572 I1 is also shown in the figure (brown dashed line). Although these RIVs do not exhibit
573 significant trends, we can observe a general agreement of the RIV between the
574 WPASH-I1 and summer O_3 concentrations in most UAs, featured by their annual
575 oscillations. **Figure 9c** shows the correlation coefficients between the RIVs of the
576 summer WPSH-I1 and O_3 concentrations. The highest correlation is found in the MYR,
577 followed by the PRD and YRD, whereas the lowest correlation occurred in the BTH.
578 These correlations suggest that the O_3 interannual fluctuations in those areas proximate
579 to the WPSH tend to be more strongly associated with the WPSH, regardless of the
580 positive or negative effect of the WPSH on O_3 evolution. This is because, as a large-
581 scale high-pressure system, the WPSH affects significantly on its surrounding weather
582 conditions, which, in turn, perturbs O_3 concentrations in its nearby regions. Since the
583 meteorology determined largely the interannual fluctuations of summer O_3 and
584 connected nicely with the WPSH, the associations of the RIVs between summer the
585 WPSH-I1 and O_3 concentrations imply that the WPSH made a stronger contribution to
586 the interannual variation of summer O_3, rather than its long-term trend, though the
587 WPSH-I1 presents an increasing trend after 1998 (**Fig. 3**).
588

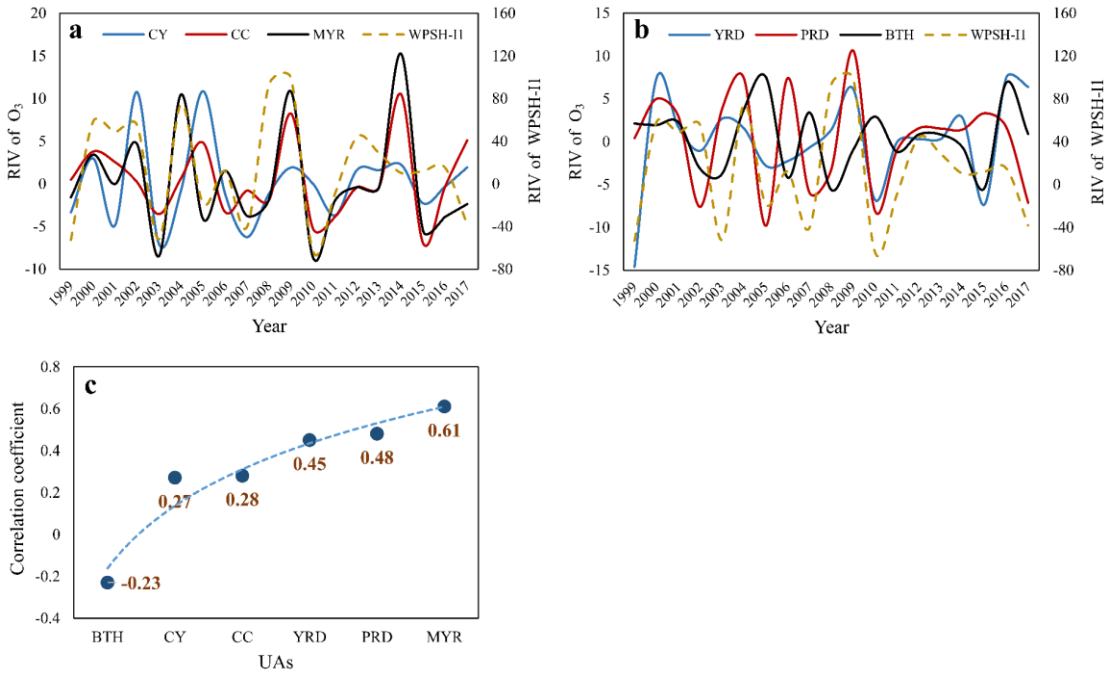

589

590 **Figure 9.** (a) Rate of interannual variations of summer WPSH-I1 (brown dashed line) and O_3 in CY,
591 CC, and MYR from 1999 to 2017, (b) same as Fig. 9a but for YRD, PRD, and BTH, and (c)
592 correlation coefficients of the rate of interannual variations of summer WPSH-I1 and O_3 in six UAs
593 from 1999 to 2017.

594

595 ## 4. Conclusions

596 Model simulations revealed higher O_3 concentrations from 1999 to 2017 in the
597 Sichuan Basin and the region extending from central China to the NCP, agreeing with
598 measured mean summer concentrations. The first EOF loadings (PCA1) are associated
599 strongly with the mean summer O_3 concentrations across China and its major UAs with
600 the correlation coefficient r=0.56 ($P \leqslant 0.01$). We identified distinctive differences
601 between positive and negative WPSH anomalies and elucidated their impacts on
602 interannual variation of O_3 and meteorological conditions. In some of the UAs, such as
603 the PRD, where relatively lower O_3 levels were reported compared to other major UAs.
604 The EOF and regression analysis revealed stronger responses of summer O_3 simulated
605 under model scenario 2 (fixed precursor emission) in the region extending from
606 southeastern to central China with the highest correlation of 0.7 in the MYR. We noted
607 that WPSH became stronger since the late 1990s and early 2000s, featured by the
608 enhancing WPSH index after 1999. As a result, stronger associations between summer

O_3 in China and its primary UAs and the WPSH occurred in the recent two decades. Extensive model scenario simulations indicated that precursor emissions dominated the long-term trend and magnitude of summer ozone concentrations. However, the meteorology associated with the WPSH largely determined their interannual fluctuations from 1999 to 2017, demonstrated by the positive correlation coefficients between RIV and WPSH-I1 in China's major UAs (except for BTH), ranging from 0.27 to 0.61. Our results concluded that the influence of precursor emissions on the evolution of ozone was stronger in Chengdu-Chongqing, the middle reaches of the Yangtze River, and central China than in the coastal city clusters. However, the influence of meteorological conditions is not significant. In contrast, for the coastal city clusters of the Yangtze River Delta, the Pearl River Delta, and the Beijing-Tianjin-Hebei region, the influence of precursor emissions on the summer ozone evolution is weaker than in the inland city clusters, but the influence of meteorological conditions was greater than in the inland city clusters, particularly in those urban areas proximate to the WPSH. Considering the great efforts in China to mitigate O_3 pollution via reducing anthropogenic precursor emissions, interannual and longer-term O_3 evolutions associated with increasing WPSH strength might be worth paying attention because it might influence background O_3 concentration, its long-term prediction, and long-term O_3 mitigation measures. The results from the present study might also imply that the local policy makers in different UAs should take the WPSH's impacts into account in making their respective O_3 reduction strategies, in addition to precursor emissions. To the end, it is worth noting that this modeling study was partly based on an increasing trend of the summer WPSH strength since 2000, which coincided with growing O_3 evolution. Historically, the WPSH has been fluctuated on a yearly basis. Further study needs to be conducted to discern the associations between projected WPSH and O_3 concentrations subject to future climate change scenarios, such as shared socioeconomic pathways under Coupled Model Intercomparison Project (CMIP6) and the Intergovernmental Panel on Climate Change (O'Neill et al., 2017).

Code/Data availability

Data will be made available on request.

Author contributions

All authors contributed to the manuscript and have given approval of the final version. XZ, RZ and XJ designed the research. XZ, XL and KC collected the data. ST, JL, HG and TH contributed to the interpretation of results. XZ, RZ and JM wrote and revised the manuscript.

Competing interests

The authors declare that they have no known competing financial interests or personal relationships that could have appeared to influence the work reported in this paper.

Financial support

This study is supported by the National Natural Science Foundation of China (41991312, 41977357).

Appendix A. Supplementary data

Supplementary data to this article can be found online

References

Akimoto, H., Mori, Y., Sasaki, K., Nakanishi, H., Ohizumi, T., and Itano, Y.: Analysis of monitoring data of ground-level ozone in Japan for long-term trend during 1990–2010: Causes of temporal and spatial variation, Atmos. Environ., 102, 302–310, https://doi.org/10.1016/J.ATMOSENV.2014.12.001, 2015.

Bell, M. L., Zanobetti, A., and Dominici, F.: Who is more affected by ozone pollution? A systematic review and meta-analysis, American Journal of Epidemiology, 180, 15–28, https://doi.org/10.1093/aje/kwu115, 2014.

Brauer, M., Amann, M., Burnett, R. T., Cohen, A., Dentener, F., Ezzati, M., Henderson, S. B., Krzyzanowski, M., Martin, R., van Dingenen, R., van Donkelaar, A., and Thurston, G. D.: Exposure assessment for estimation of the global burden of disease attributable to outdoor air pollution, Environ. Sci. Technol., 46, 652–660, https://doi.org/10.1021/es2025752, 2012.

Chen, Z., Li, R., Chen, D., Zhuang, Y., Gao, B., Yang, L., and Li, M.: Understanding the causal influence of major meteorological factors on ground ozone concentrations across China, J. Clean. Prod., 242, 118498, https://doi.org/10.1016/j.jclepro.2019.118498, 2020.

Dang, R., Liao, H., and Fu, Y.: Quantifying the anthropogenic and meteorological influences on summertime surface ozone in China over 2012–2017, Sci. Total Environ., 754, 142394, https://doi.org/10.1016/j.scitotenv.2020.142394, 2021.

Ding, D., Xing, J., Wang, S., Chang, X., and Hao, J.: Impacts of emissions and meteorological

changes on China's ozone pollution in the warm seasons of 2013 and 2017, Front. Environ. Sci. Eng., 13, 76, https://doi.org/10.1007/s11783-019-1160-1, 2019.

Duan, L., Rong, Y., and Liang, P.: Effect of West Pacific Subtropical High on Summer Precipitation in North China, Met. Sci. Technol., 36, 273–276, http://www.cnki.com.cn/Article/CJFDTotal-QXKJ200803004.htm, 2008.

Fiore, A. M., Jacob, D. J., Mathur, R., and Martin, R. V.: Application of empirical orthogonal functions to evaluate ozone simulations with regional and global models, J. Geophys. Res. Atmos., 108, https://doi.org/10.1029/2002jd003151, 2003.

Fleming, Z. L., Doherty, R. M., von Schneidemesser, E., Malley, C. S., Cooper, O. R., Pinto, J. P., Colette, A., Xu, X., Simpson, D., Schultz, M. G., Lefohn, A. S., Hamad, S., Moolla, R., Solberg, S., and Feng, Z.: Tropospheric Ozone Assessment Report: Present-day ozone distribution and trends relevant to human health, Elementa, 6, 12, https://doi.org/10.1525/elementa.273, 2018.

Fu, Y., Liao, H., and Yang, Y: Interannual and Decadal Changes in Tropospheric Ozone in China and the Associated Chemistry-Climate Interactions: A Review, Adv. Atmos. Sci., 36, 975–993, https://doi.org/10.1007/s00376-019, 2019.

Guenther, A. B., Jiang, X., Heald, C. L., Sakulyanontvittaya, T., Duhl, T., Emmons, L. K., and Wang, X.: The Model of Emissions of Gases and Aerosols from Nature version 2.1 (MEGAN2.1): an extended and updated framework for modeling biogenic emissions, Geosci. Model Dev., 5, 1471–1492, https://doi.org/10.5194/gmd-5-1471-2012, 2012.

Han, H., Liu, J., Shu, L., Wang, T., and Yuan, H.: Local and synoptic meteorological influences on daily variability in summertime surface ozone in eastern China, Atmos. Chem. Phys., 20, 203–222, https://doi.org/10.5194/acp-20-203-2020, 2020.

Huang, Y., Wang, B., Li, X., and Wang, H.: Changes in the influence of the western Pacific subtropical high on Asian summer monsoon rainfall in the late 1990s, Clim. Dyn., 51, 443–455, https://doi.org/10.1007/s00382-017-3933-1, 2018.

Jiang, Z., Li, J., Lu, X., Gong, C., Zhang, L., and Liao, H.: Impact of western Pacific subtropical high on ozone pollution over eastern China, Atmos. Chem. Phys., 21, 2601–2613, https://doi.org/10.5194/acp-21-2601-2021, 2021.

Lefohn, A. S., Malley, C. S., Simon, H., Wells, B., Xu, X., Zhang, L., and Wang, T.: Responses of human health and vegetation exposure metrics to changes in ozone concentration distributions in the European Union, United States, and China, Atmos. Environ., 152, 123–145, https://doi.org/10.1016/j.atmosenv.2016.12.025, 2017.

Li, K., Jacob, D. J., Liao, H., Shen, L., Zhang, Q., and Bates, K. H.: Anthropogenic drivers of 2013–2017 trends in summer surface ozone in China, Proc. Natl. Acad. Sci. U. S. A., 116, 422–427, https://doi.org/10.1073/pnas.1812168116, 2019.

Li, K., Jacob, D.J., Shen, L., Lu, X., de Smedt, I., and Liao, H.: Increases in surface ozone pollution in China from 2013 to 2019: Anthropogenic and meteorological influences, Atmos. Chem. Phys., 20, 11423–11433, https://doi.org/10.5194/acp-20-11423-2020, 2020.

Lin, C. Q., Lau, A. K. H., Fung, J. C. H., Song, Y. S., Li, Y., Tao, M. H., Lu, X. C., Ma, J., and Lao, X. Q.: Removing the effects of meteorological factors on changes in nitrogen dioxide and

ozone concentrations in China from 2013 to 2020, Sci. Total Environ., 793, 148575, https://doi.org/10.1016/j.scitotenv.2021.148575, 2021.

Lin, Y., Zhang, L., Fan, Q., Meng, H., Gao, Y., Gao, H., and Yao, X.: Decoupling impacts of weather conditions on interannual variations in concentrations of criteria air pollutants in South China – constraining analysis uncertainties by using multiple analysis tools, Atmos. Chem. Phys., 22, 16073–16090, https://doi.org/10.5194/acp-22-16073-2022, 2022.

Liu, H., Liu, S., Xue, B., Lv, Z., Meng, Z., Yang, X., Xue, T., Yu, Q., and He, K.: Ground-level ozone pollution and its health impacts in China, Atmos. Environ., 173, 223–230, https://doi.org/10.1016/j.atmosenv.2017.11.014, 2018.

Liu, J.: Ozone regionalization and evolution characteristics, and meteorlogical formation mechanism in China from 2013 to 2018, Ph.D. thesis, http://cdmd.cnki.com.cn/article/cdmd-10300-1021778486.htm, 2020.

Liu, Q., Zhou, T., Mao, H., and Fu, C.: Decadal variations in the relationship between the western Pacific subtropical high and summer heat waves in east China, J. Clim., 32, 1627–1640, https://doi.org/10.1175/JCLI-D-18-0093.1, 2019a.

Liu, Y., Liang, P., and Sun, Y.: Characteristics of the Western Pacific Subtropical High and Summer Rainfall Anomalies, The Asian Summer Monsoon, 85–95, https://doi.org/10.1016/B978-0-12-815881-4.00005-6, 2019b.

Liu, Y., and Wang, T.: Worsening urban ozone pollution in China from 2013 to 2017 - Part 1: The complex and varying roles of meteorology, Atmos. Chem. Phys., 20, 6305–6321, https://doi.org/10.5194/acp-20-6305-2020, 2020.

Lu, M. H., Chen, X., Liu, W. C., Zhu, F., Lim, K. S., McInerney, C. E., and Hu, G.: Swarms of brown planthopper migrate into the lower yangtze river valley under strong western pacific subtropical highs, Ecosphere, 8, https://doi.org/10.1002/ecs2.1967, 2017.

Lu, X., Hong, J., Zhang, L., Cooper, O. R., Schultz, M. G., Xu, X., Wang, T., Gao, M., Zhao, Y., and Zhang, Y.: Severe Surface Ozone Pollution in China: A Global Perspective, Environ. Sci. Technol. Lett., 5, 487–494, https://doi.org/10.1021/acs.estlett.8b00366, 2018.

Lu, X., Zhang, L., Zhao, Y., Jacob, D. J., Hu, Y., Hu, L., Gao, M., Liu, X., Petropavlovskikh, I., McClure-Begley, A., and Querel, R.: Surface and tropospheric ozone trends in the Southern Hemisphere since 1990: possible linkages to poleward expansion of the Hadley circulation, Sci. Bull., 64, 400–409, https://doi.org/10.1016/j.scib.2018.12.021, 2019.

Ma, M., Yao, G., Guo, J., and Bai, K.: Distinct spatiotemporal variation patterns of surface ozone in China due to diverse influential factors, J. Environ. Manage., 288, 112368, https://doi.org/10.1016/j.jenvman.2021.112368, 2021.

Ma, Z., Xu, J., Quan, W., Zhang, Z., Lin, W., and Xu, X.: Significant increase of surface ozone at a rural site, north of eastern China, Atmos. Chem. Phys., 16, 3969–3977, https://doi.org/10.5194/acp-16-3969-2016, 2016.

Maji, K. J., Ye, W. F., Arora, M., and Nagendra, S. M. S.: Ozone pollution in Chinese cities: Assessment of seasonal variation, health effects and economic burden, Environ. Pollut., 247, 792–801, https://doi.org/10.1016/j.envpol.2019.01.049, 2019.

758 Monks, P. S., Archibald, A. T., Colette, A., Cooper, O., Coyle, M., Derwent, R., Fowler, D., Granier,
759 C., Law, K. S., Mills, G. E., Stevenson, D. S., Tarasova, O., Thouret, V., von Schneidemesser,
760 E., Sommariva, R., Wild, O., and Williams, M. L.: Tropospheric ozone and its precursors from
761 the urban to the global scale from air quality to short-lived climate forcer, Atmos. Chem. Phys.,
762 https://doi.org/10.5194/acp-15-8889-2015, 2015.

763 Nie, J., Liu, P., and Zhao, C.: Research on Relationship between Various Indexes of the Western
764 North Pacific Subtropical High and Summer Precipitation in Eastern China, Chinese Journal
765 of Atmospheric Sciences, 45, 833–850, https://doi.org/10.3878/j.issn.1006-9895.2009.20160,
766 2021.

767 O'Neill, B. C., Kriegler, E., Ebi, K. L., Kemp-Benedict, E., Riahi, K., Rothman, D. S., van Ruijven,
768 B. J., van Vuuren, D. P., Birkmann, J., Kok, K., Levy, M., and Solecki, W.: The roads ahead:
769 Narratives for shared socioeconomic pathways describing world futures in the 21st century,
770 Global Environmental Change, 42, 169–180, https://doi:10.1016/j.gloenvcha.2015.01.004,
771 2017.

772 Pu, B., Dickinson, R. E., and Fu, R.: Dynamical connection between Great Plains low-level winds
773 and variability of central Gulf States precipitation, J. Geophys. Res., 121, 3421–3434,
774 https://doi.org/10.1002/2015JD024045, 2016.

775 Shen, L., Mickley, L. J., and Tai, A. P. K.: Influence of synoptic patterns on surface ozone variability
776 over the eastern United States from 1980 to 2012, Atmos. Chem. Phys., 15, 10925–10938,
777 https://doi.org/10.5194/acp-15-10925-2015, 2015.

778 Silva, R. A., West, J. J., Zhang, Y., Anenberg, S. C., Lamarque, J. F., Shindell, D. T., Collins, W. J.,
779 Dalsoren, S., Faluvegi, G., Folberth, G., Horowitz, L. W., Nagashima, T., Naik, V., Rumbold,
780 S., Skeie, R., Sudo, K., Takemura, T., Bergmann, D., Cameron-Smith, P., Cionni, I., Doherty,
781 R. M., Eyring, V., Josse, B., MacKenzie, I. A., Plummer, D., Righi, M., Stevenson, D. S., Strode,
782 S., Szopa, S., and Zeng, G.: Global premature mortality due to anthropogenic outdoor air
783 pollution and the contribution of past climate change, Environ. Res. Lett., 8, 034005,
784 https://doi.org/10.1088/1748-9326/8/3/034005, 2013.

785 Su, T., Xue, F., and Zhang, H.: Simulating the intraseasonal variation of the East Asian summer
786 monsoon by IAP AGCM4.0, Adv. Atmos. Sci., 31, 570–580, https://doi.org/10.1007/s00376-
787 013-3029-8, 2014.

788 Wang, Y., Jia, B., Wang, S. C., Estes, M., Shen, L., and Xie, Y.: Influence of the Bermuda High on
789 interannual variability of summertime ozone in the Houston–Galveston–Brazoria region,
790 Atmos. Chem. Phys., 16, 15265–15276, https://doi.org/10.5194/acp-16-15265-2016, 2016.

791 Wu, D., Fung, J., Yao, T., and Lau, A.: A study of control policy in the Pearl River Delta region by
792 using the particulate matter source apportionment method, Atmos. Environ., 76, 147-161,
793 https://doi.org/10.1016/j.atmosenv.2012.11.069, 2013.

794 Xu, W., Lin, W., Xu, X., Tang, J., Huang, J., Wu, H., and Zhang, X.: Long-term trends of surface
795 ozone and its influencing factors at the Mt Waliguan GAW station, China-Part 1: Overall trends
796 and characteristics, Atmos. Chem. Phys., 16, 6191–6205, https://doi.org/10.5194/acp-16-6191-
797 2016, 2016.

798 Yan, M., Liu, Z., Liu, X., Duan, H., and Li, T.: Meta-analysis of the Chinese studies of the

799 association between ambient ozone and mortality, Chemosphere, 93, 899–905,
800 https://doi.org/10.1016/j.chemosphere.2013.05.040, 2013.

801 Yang, K., Cai, W., Huang, G., Hu, K., Ng, B., and Wang, G.: Increased variability of the western
802 Pacific subtropical high under greenhouse warming, Proc. Natl. Acad. Sci. U. S. A., 119,
803 e2120335119, https://doi.org/10.1073/pnas, 2022.

804 Yihui, D., and Chan, J.: The East Asian summer monsoon: An overview, Meteorology and
805 Atmospheric Physics, 89,117–142, https://doi.org/10.1007/s00703-005-0125-z, 2005.

806 Yin, Z., Cao, B., and Wang, H.: Dominant patterns of summer ozone pollution in eastern China and
807 associated atmospheric circulations, Atmos. Chem. Phys., 19, 13933–13943,
808 https://doi.org/10.5194/acp-19-13933-2019, 2019.

809 Zhan, Y., Luo, Y., Deng, X., Grieneisen, M. L., Zhang, M., and Di, B.: Spatiotemporal prediction of
810 daily ambient ozone levels across China using random forest for human exposure assessment,
811 Environ. Pollut., 233, 464–473, https://doi.org/10.1016/j.envpol.2017.10.029, 2018.

812 Zhang, X., Jian, X., Zhao, Y., Liu, X., Chen, K., Wang, L., Tao, S., Liu, J., Huang, T., Gao, H., Liu,
813 Y., Zhugu, R., and Ma, J.: Tropospheric Ozone Perturbations Induced by Urban Land
814 Expansion in China from 1980 to 2017, Environ. Sci. Technol., 56, 6978–6987,
815 https://doi.org/10.1021/acs.est.1c06664, 2022.

816 Zhao, Z., and Wang, Y.: Influence of the West Pacific subtropical high on surface ozone daily
817 variability in summertime over eastern China, Atmos. Environ., 170, 197–204,
818 https://doi.org/10.1016/j.atmosenv.2017.09.024, 2017.

819 Zhou, T., Yu, R., Zhang, J., Drange, H., Cassou, C., Deser, C., Hodson, D. L. R., Sanchez-Gomez,
820 E., Li, J., Keenlyside, N., Xin, X., and Okumura, Y.: Why the Western Pacific subtropical high
821 has extended westward since the late 1970s, J. Clim., 22, 2199–2215,
822 https://doi.org/10.1175/2008JCLI2527.1, 2009.

823